09 Feb 2024

PISA Printing Microneedles With Controllable Aqueous Dissolution Kinetics

Aaron Priester

Jimmy Yeng

Yuwei Zhang

Krista Hilmas

et. al. For a complete list of authors, see https://scholarsmine.mst.edu/chem_facwork/3679

Recommended Citation

A. Priester et al., "PISA Printing Microneedles With Controllable Aqueous Dissolution Kinetics," *ACS Applied Polymer Materials*, vol. 6, no. 3, pp. 1944 - 1950, American Chemical Society, Feb 2024.
The definitive version is available at https://doi.org/10.1021/acsapm.3c02796

ACS APPLIED POLYMER MATERIALS

pubs.acs.org/acsapm Article

PISA Printing Microneedles with Controllable Aqueous Dissolution Kinetics

Aaron Priester, Jimmy Yeng, Yuwei Zhang, Krista Hilmas, Risheng Wang, and Anthony J. Convertine*

Cite This: ACS Appl. Polym. Mater. 2024, 6, 1944−1950 Read Online

ACCESS | Metrics & More | Article Recommendations | Supporting Information

ABSTRACT: This study focused on the development of high-resolution polymeric structures using polymer-induced self-assembly (PISA) printing with commercially available digital light-processing (DLP) printers. Significantly, soluble solids could be 3D-printed using this methodology with controllable aqueous dissolution rates. This was achieved using a highly branched macrochain transfer agent (macro-CTA) containing multiple covalently attached CTA groups. In this work, the use of acrylamide as the self-assembling monomer in isopropyl alcohol was explored with the addition of N-(butoxymethyl)acrylamide to modulate the aqueous dissolution kinetics. PISA-printed microneedles were observed to have feature sizes as small as 27 μm, which was close to the resolution limit of the DLP printer. Atomic force measurements confirm the presence of a complex mixture of PISA morphologies, including spheres and worms. Additionally, "poke and release" microneedles were fabricated; their base dissolved rapidly in physiological fluids, leaving behind more slowly dissolving tips, thereby demonstrating the potential for sustained drug delivery.

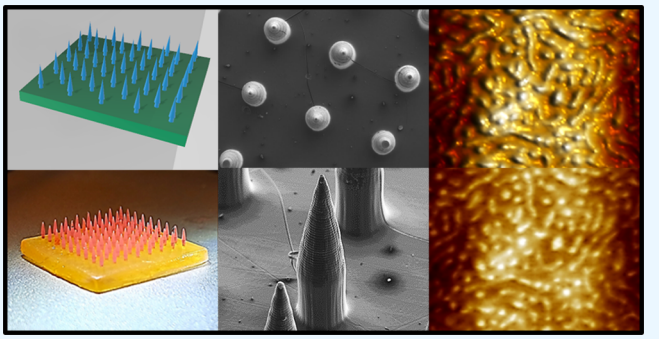

KEYWORDS: *PISA printing, RAFT, soluble solids, DLP, 3D printing*

INTRODUCTION

Digital light processing (DLP) 3D printers are known for high resolution and have been used extensively in biomedical engineering, particularly in the fabrication of microfluidic devices.[1−3] However, these traditional methods often lack precise control over polymer architecture, a limitation addressed by reversible deactivation radical polymerization (RDRP) techniques.[4−7] Reversible addition−fragmentation chain transfer (RAFT) polymerization, a subset of RDRP, has gained attention for its applications in 3D printing. Boyer et al. demonstrated the use of RAFT for 3D and 4D prints, achieving rapid polymerization and build speeds.[8−10] Other researchers have similarly applied RAFT-based photopolymerization in DLP printing, offering improvements in mechanical properties and glass transition temperatures.[11−14] RAFT techniques also enhance thermomechanical properties and allow for postmodification capabilities that are not feasible with traditional methods.[15,16] We recently reported the development of RAFT polymerization-induced self-assembly (RAFT PISA) printing, which allows parts to be 3D printed without the need for multifunctional cross-linking monomers.[17] This methodology yields parts that are stabilized by physical rather than chemical cross-links. Similar to conventional PISA, PISA printing employs a RAFT macrochain transfer agent (macro-CTA) that is chain extended with a monomer that phase separates during block copolymer formation. However, in order to PISA print mechanically stable parts, we have found that at least two CTA residues should be attached to the macro-CTA.

Our initial PISA printing study employed a DLP printer to PISA print diacetone acrylamide (DAAm) from a difunctional poly(ethylene glycol) (PEG) macro-CTA in water with lithium phenyl-2,4,6-trimethylbenzoylphosphinate (LAP) and phenol red functioning as the photoinitiator and photoabsorber, respectively. Significantly, PISA-printed parts prepared from these resins dissolved completely in N,N-dimethylformamide (DMF). Atomic force microscopy (AFM) analyses of these structures revealed morphologies consisting of interconnected PISA nanostructures. These nanostructural domains closely resemble those in another DLP printing system based on RAFT polymerization-induced microphase separation (PIMS), in studies by Boyer et al. and company.[18,19] The development and evolution of the nanostructural features or domains with degree of polymerization in PIMS mirrors those typically observed in PISA systems. Their system was based on

Received: November 15, 2023
Revised: January 1, 2024
Accepted: January 3, 2024
Published: January 24, 2024

https://doi.org/10.1021/acsapm.3c02796
ACS Appl. Polym. Mater. 2024, 6, 1944−1950

polymerization-induced phase separation in bulk monomer with chemical cross-linking agents being included to lock in the nanophase-separated regions. While these materials have significant advantages in mechanical properties, they suffer from long cure times (180 s/layer) and lack degradability. The PISA printing systems, in contrast, have displayed reduced cure times (<60 s/layer). They can also be designed to dissolve in specific solvents such as water following printing yet can remain stable and retain their shapes and nanostrucural features in the photopolymerization solvent. This makes these systems intriguing for fields such as drug delivery and tissue engineering in which controlled dissolution could be advantageous. In the present work, we aimed to develop PISA printing resins that could be engineered to dissolve at controllable rates under physiological conditions. Herein, we detail the development of PISA printing resins based on the self-assembly of acrylamide in isopropanol.

The goals of this study were 3-fold: first, to assess the ability to create high-resolution objects using the PISA printing method; second, to confirm that these objects are not cross-linked and can dissolve in suitable solvents; and third, to create resin mixtures that print well in organic solvents such as isopropanol but can also dissolve at controlled rates under physiological conditions. In our previous PISA printing study, we found that the use of macro-CTAs with multiple RAFT CTAs is crucial for achieving the mechanical strength necessary to PISA print objects with a DLP printer.[17] We hypothesize that the mechanical stability of the printed objects arises from a combination of interparticle bridging and knotting among the soluble corona-stabilizing segments (Figure 1A,B). To prepare macro-CTAs with multiple covalently bound CTAs, we first homopolymerized a RAFT transmer to produce a highly branched polymer. From this core, we then homopolymerized N,N-dimethylacrylamide (DMA) to yield radiant star scaffolds (RSSs) in which linear DMA segments radiate outward from a central highly branched core (Figure 1C). Here, a monomer-to-CTA-to-initiator ([M]0:[CTA]0:[I]0) ratio of 100:1:0.05 was employed for the polymerization which was conducted in DMF at 70 °C for 24 h.

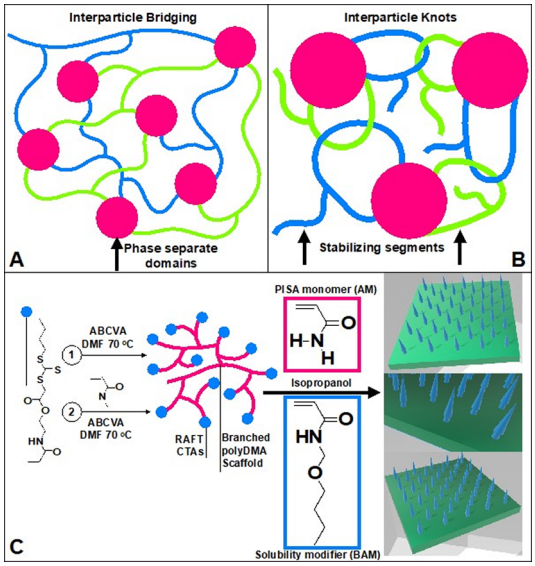

Figure 1. Mechanisms of physical cross-linking that allow PISA resins to be DLP printed are thought to result from (A) interparticle bridging and (B) interparticle knots. These PISA resins employ a branchy homopolymerized transmer scaffold as the macro-CTA stabilizing segments. (C) Transmers were homopolymerized and then chain extended with DMA to form RSSs. These macro-CTAs were then employed in an AM-based PISA system in isopropanol, along with BAM solubility modifier, to make 3D DLP PISA resins for printing microneedle scaffolds.

RESULTS AND DISCUSSION

GPC analysis of the homopolymerized transmer and the corresponding poly(DMA) RSS indicated broad molecular weight distributions and relatively low molecular weights, which is consistent with previous studies employing thermal polymerization conditions.[20] The molecular weight and molar mass dispersity of the poly(DMA) RSS were determined to be 28,443 g/mol and 2.00, respectively. The homopolymerized transmer molecular weight was determined to be approximately 3000 Da; however, the broad multimodal distribution complicated the determination of the molecular weight. Due to the highly branched nature of these polymers, the molecular weights, which are based on linear polystyrene standards, likely underestimate their true values. For this reason, the CTA concentration for subsequent PISA printing experiments was determined via UV vis spectroscopy at 325 nm based on the extinction coefficient of the starting CTA (Supporting Information Figure 1). ^{1}H NMR and GPC of synthesized homopolymerized transmer and poly(DMA) RSS can be found in the Supporting Information Figures 2−8.

The next stage of this study was focused on developing a PISA printing resin formulation that could be printed in isopropyl alcohol and yield parts with controllable dissolution rates under aqueous conditions. The choice of isopropyl alcohol as the polymerization medium was influenced by several factors, such as its high boiling point, cost-effectiveness, low toxicity, and wide availability. Extensive literature exists on alcoholic RAFT dispersion polymerizations using various monomers such as styrene,[21−27] benzyl methacrylate,[28−32] and other methacrylates with aromatic groups;[33−35] however, these typically produce materials with limited solubility in water. To overcome this limitation, acrylamide (AM) was selected as the phase-separating monomer due to its high solubility in isopropyl alcohol and its ability to produce water-soluble hydrophilic polymers. To fine-tune the dissolution kinetics of the resulting PISA-printed structures in aqueous media, a hydrophobic monomer, N-(butoxymethyl)acrylamide (BAM), was added to the formulation. Our hypothesis was that including BAM at low feed ratios would neither interfere with the self-assembly process nor compromise structural integrity while effectively controlling the aqueous dissolution rates of the structures. While BAM was employed in these studies, monomers such as DAAM (diacetone acrylamide) or BA (butyl acrylate) could also potentially be employed in place of BAM to slow dissolution.

Prior to the PISA printing experiments, we systematically studied the effect of both the core-forming segment DP and the AM-to-BAM molar ratio. Here, the goal was to determine how these variables affect the aqueous dissolution kinetics of the polymerized materials. In these experiments, cylindrical samples were prepared via bulk photopolymerization in cylindrical molds with a diameter of 14 mm and a resin weight of 1.5 g. The cured samples were then placed in phosphate-buffered saline (PBS) at a temperature of 37 °C to study their dissolution behavior. Shown in Figure 2A are the

https://doi.org/10.1021/acsapm.3c02796
ACS Appl. Polym. Mater. 2024, 6, 1944−1950

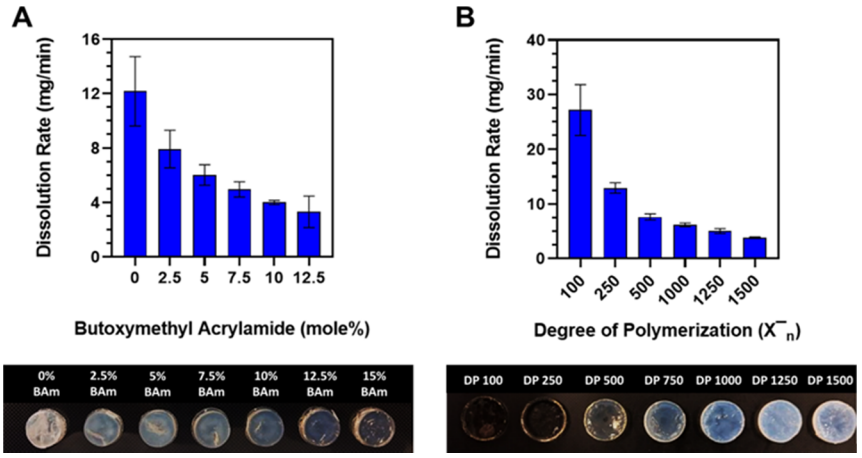

Figure 2. (a) Dissolution rate of PISA-cured resins as a function of increasing mole fraction of BAM relative to AM in the fixed DP 1000 core-forming block. Increasing amounts of hydrophobic BAM in the core-forming block slowed the dissolution rate of PISA-cured parts in water up to a value of 12.5 mol %. Increasing BAM relative to AM also decreased the blue color in the parts on account of poly(BAM) being isopropanol soluble. Parts with increasing BAM content were also more rubbery and far less brittle. (b) Dissolution rate of PISA-cured parts as a function of increasing DP of the core-forming block at a fixed molar composition of 95 mol % AM and 5 mol % BAM. Increasing target DP values decreased the rate of dissolution of the PISA-cured parts in water. Increasing DP also increased opacity from nearly transparent to almost white. This indicates the formation of PISA-based nanostructures. These nanostructures scatter light, thus making the parts appear opaque.

results of the aqueous dissolution studies for these samples. Here, the introduction of only 5 mol % BAM to AM yielded a 50% reduction in the aqueous dissolution kinetics. When the BAM content was increased to 12.5 mol %, the dissolution rate further decreased to one-fourth that of the pure AM samples. Further increases in the BAM content to 15 mol % yielded samples that did not completely dissolve but did swell and break up into pieces. These studies collectively occurred over a period of 1−1.5 h for these sample sizes. When part size (mass) was approximately doubled for all compositions, the dissolution rate was extended up to 3−3.5 h in some cases. However, the average mass loss rate for the larger-scale studies closely matched the values shown for small-scales studies in Figure 2.

In Figure 2B, the dissolution rates of samples with a fixed comonomer composition of 95 mol % AM and 5 mol % BAM are plotted against various target DPs. For the sample with a target DP of 100, the dissolution rate was the highest, estimated to be around 27 mg of mass loss per minute. As we moved to a higher target DP of 500, the dissolution rate noticeably decreased to roughly 6 mg/min. The most significant reduction in the dissolution rate was observed for the sample with a DP of 1500, where the rate was approximately 2.5 mg/min. This trend underscores the inverse relationship between the target DP and the dissolution rate, emphasizing the importance of the polymer chain length in controlling the aqueous dissolution behavior of the material. The photopolymerized samples also show a distinct difference in their appearance as a function of both the target DP as well as the molar feed ratio of AM and BAM (Figure 2A,B). Here, a transition from white to blue is observed as the composition changes completely from AM to 15 mol % BAM. This is not surprising given the solubility of BAM and its corresponding polymer in isopropanol. Similarly, a color change from clear to blue is observed as a function of target DP at a molar feed ratio of 95 mol % AM:5 mol % BAM. For example, samples cured at this position targeting a DP of 100 appear almost clear while samples prepared targeting a DP of 1500 appear blue.

Based on these findings, we next attempted to PISA print "poke and release" microneedles, in which the base is first printed using a resin composition that is designed to degrade rapidly following insertion under the skin. This leaves behind microneedle tips with compositions that dissolve more slowly. Microneedle platform supports were printed with resins formulated using 100% AM for the core-forming block (target DP of 1000) and the DP 250 DMA RSS macro-CTA. RSSs with longer DMA segments were employed in these studies because they were observed to produce a rubbery platform, which is easier to remove from the build plate. Target DPs of 500 and 750 for the AM PISA could alternatively be used as well to further reduce the stiffness of the platform, further aiding in part removal. After the bases were PISA-printed, the resin was changed to 87.5 mol % AM and −12.5 mol % BAM with a target DP of 1250. This composition was selected in order to yield microneedle tips that dissolve more slowly in water. This design offers a potential pathway for the sustained delivery of drugs, vaccines, or biologics. Alternatively, a composition of 95 mol % AM and 5 mol % BAM could also be used, although this would yield microneedle tips that would dissolve more rapidly (as indicated in Figure 2). This composition held the advantage of being stiffer, which is more ideal for microneedles. Microneedles employing this composition were printed and subsequently used for SEM imaging. Beyond the composition-dependent dissolution studies, these experiments allowed us to investigate the resolution limit of these PISA printing resins by using a commercial DLP printer with a resolution limit (XY) of 22 μm. Microneedle scaffolds were printed on the Phrozen Sonic Mini 8K printer using 25 μm layer thicknesses and normal/bottom exposure times or cure times per layer of 45−60 s.

To achieve the highest possible resolution, we added phenol red as a photoabsorber to the resins. Although it has been shown that trithiocarbonates can function effectively as photoabsorbers,[34] in these formulations, it was found that the highest resolution was obtained at a phenol red concentration of 0.01−0.02 wt % relative to total solids at pH 6. Microneedle dissolution tests were conducted in PBS at

https://doi.org/10.1021/acsapm.3c02796
ACS Appl. Polym. Mater. 2024, 6, 1944−1950

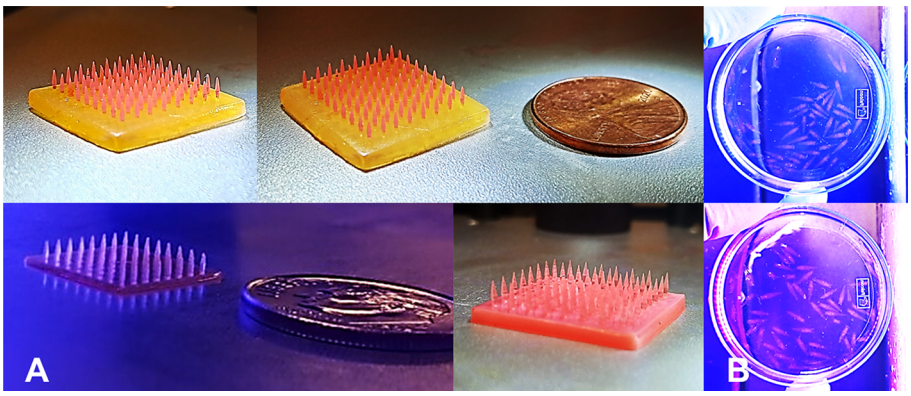

Figure 3. (A) DLP-printed microneedles by using PISA-based RSS resins. As shown, the yellow platform was printed with a PISA resin based on 100% AM DP 1000 PISA block, while the REMA-containing microneedles were printed with a PISA resin based on 90 AM−10 BAM (mole %) DP 1250 block. These microneedle scaffolds were used for base dissolution studies, leaving behind the tips shown in (B). The fully pink PISA-printed microneedles on the bottom in (A) were printed using a composition of 95 mol % AM and 5 mol % BAM in isopropanol. Those microneedle scaffolds were subsequently used for SEM imaging. (B) Microneedles in 1x PBS following the dissolution of the platform supporting them. Microneedles swell considerably in size before dissolving fully unless the formulation was altered to include cross-linker.

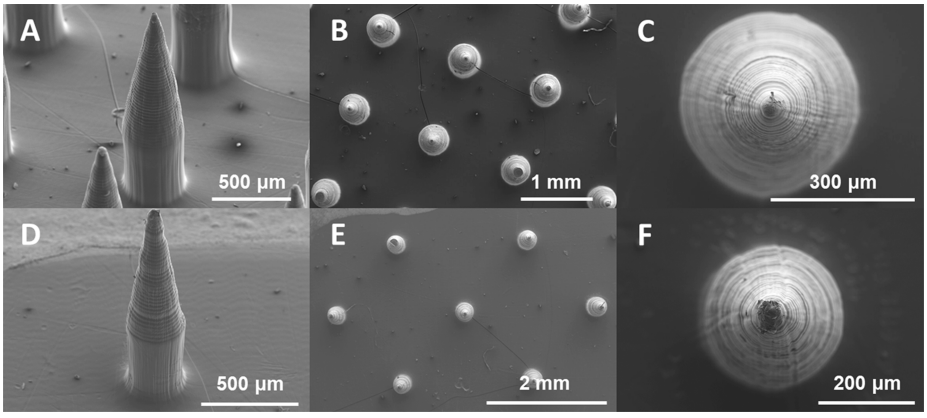

Figure 4. (A−C) Horizontal/vertical orientation and (D−F) diagonal orientation. A and D show 25 μm print layers on microneedle sides; C and F from the top are concentric circles. Larger microneedles (A) have more uniform layering than smaller ones (B) with surface inconsistencies. B and E show microcracks possibly from isopropanol evaporation. Horizontal/vertical microneedles average a 1.17 mm length, 375 μm base diameter, and 34 μm tip diameter. Diagonally arranged ones average a 927 μm length, 290 μm base diameter, and 27 μm tip diameter. Tip diameters are near the 22 μm XY resolution limit of the Phrozen Sonic Mini 8K printer, indicating the suitability for skin penetration.

37 °C. In these studies, the platforms were observed to dissolve in approximately 15 min, leaving behind the microneedle tips. Here, a small quantity of rhodamine B methacrylate was incorporated into the tips to make them easier to visualize. Shown in Figure 3A are images showing the microneedles printed under these conditions. The platforms, printed in the absence of the rhodamine B methacrylate, appear yellow, while the tips, which included the fluorescent monomer, appear pink. The all-pink microneedle scaffolds shown in the bottom of Figure 3A were printed fully with a targeted composition of 95 mol % AM and 5 mol % BAM and were used for SEM imaging. Following the dissolution of the bases, the tips can be observed (Figure 3B). The printed microneedle scaffold dimensions closely matched those of the CAD design, and the features were nearly identical those in the CAD file.

Based on this resin composition, the tips would then dissolve shortly after within an hour. It was, however, also possible to PISA print tips that swell but do not dissolve with the incorporation of a small amount of N′*N*-Methylenebis-(acrylamide) (e.g., 1.5 wt %) cross-linker or by adjusting the composition to 85 mol % AM and 15 mol % BAM. At this target compositional ratio, the PISA resins will swell but not dissolve. Microneedles with cross-linker will remain intact indefinitely unless broken down, which can happen in the case of enzymatic degradation via proteases in the body. Compositions of 15 mol % or greater BAM did not seem to break down further in subsequent weeks and were quite stable. Since there were no chemical cross-links that could be broken down via enzymatic degradation, these parts would likely remain intact. Microneedles underwent a scanning electron microscopy (SEM) examination to assess their tip dimensions. Figures 4A−C display SEM images of microneedles in a horizontal/vertical arrangement, with Figure 4B focusing on a microneedle with a larger intended dimension. Figure 4D−F, on the other hand, illustrates microneedles arranged diagonally, with Figure 4E highlighting a microneedle of a smaller intended size. The 25 μm print layers are visible as lines on the sides of the microneedles (Figure 4A,D) and as concentric circles when viewed from the top (Figure 4C,F). Microneedles with larger dimensions (Figure 4A) display more uniform layering and smoother surfaces than the smaller ones (Figure 4B), which exhibit some inconsistencies on their surfaces, particularly on the diagonal of the cone. Some microneedles, as seen in Figure 4B,E, also show microcracks,

https://doi.org/10.1021/acsapm.3c02796
ACS Appl. Polym. Mater. 2024, 6, 1944−1950

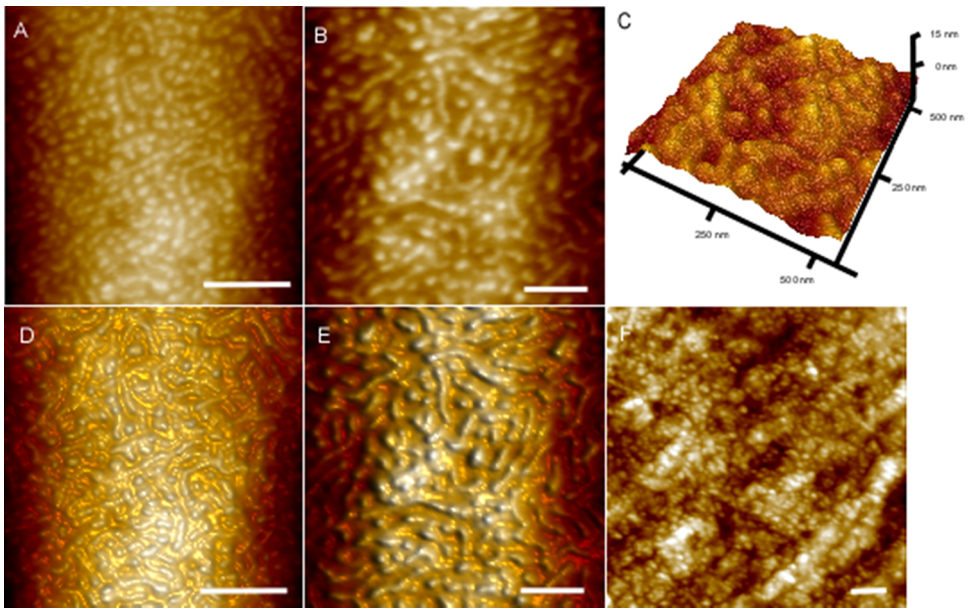

Figure 5. AFM characterization of PISA printing resins: (A) AFM topography image of cured PISA resin containing 0.1 wt % LAP photoinitiator with respect to solids, (B) AFM topography image of cured PISA resin containing 0.1 wt % LAP with respect to solids and a target DP of 500, (C) AFM 3D view of the cured sample with 0.1 wt % LAP, and (D–F) AFM 2D topography images of the cured samples with 0.1 wt % LAP, respectively. Scale bar: 150 nm.

which may have been caused by stresses from the swift evaporation of isopropanol.

Analysis using ImageJ software indicates that microneedles in the horizontal/vertical configuration have an average length of 1.17 ± 0.023 mm, a base diameter of 375 ± 3.71 μm, and a tip diameter of 34 ± 1.8 μm. In contrast, the diagonally arranged microneedles have a length of 927 ± 12.2 μm, a base diameter of 290 ± 2.5 μm, and a tip diameter of 27 ± 3.5 μm. It is noteworthy that the tip diameters align well with the XY resolution limit of the Phrozen Sonic Mini 8K printer, which is 22 μm. When compared with conventional hypodermic needles, these microneedle tips have narrower widths, indicating their suitability for skin penetration. AFM measurements were conducted to examine the surface morphology of the PISA-printed objects (Figure 5). Roughness and topographical imaging of the part surface reveals the presence of wormlike particles, spherical particles, and/or phase-separated domains, which may be a direct consequence of the self-assembly process during printing/curing. These observations are consistent with the proposed mechanism for PISA printing.

While the objective of these studies was not to demonstrate the biological activity of the PISA-printed microneedles, we did want to highlight the ability to release small molecules from the 3D-printed structures. Here, two different loading strategies were employed: (1) a polymerizable prodrug based on 10-hydroxycamptothecin was introduced into the RSS during the polymerization of the DMA stabilizing segment and (2) methylene blue trihydrate (MBT) was encapsulated within the microneedles in the PISA printing process. The former approach leads to polymeric prodrugs, wherein the drug is anchored to the polymer scaffold through a hydrolytically cleavable phenyl ester. Postdissolution of the PISA-printed needle tips within the body, the polymer then gradually releases the covalently attached drug. In the latter method, MBT is physically confined within the PISA-printed tip, facilitating its swift release upon needle tip dissolution.

To streamline the quantification of the 10CAM drug release, a small amount of cross-linker was integrated into the PISA printing resin, ensuring the needle tips did not dissolve entirely. This allowed accurate absorbance measurements for the drug to be taken without interference from the polymer. Microneedles containing 10CAM residues released 6% of the drug over a period of 8 h (Supporting Information Figure 9A). These kinetics are consistent with our previous studies of this monomer. In comparison, 22% of MBT was released into the surrounding PBS over a period of 4 h (Supporting Information Figure 9B). Microneedles PISA printed in the absence of the cross-linker showed nearly instantaneous release of the encapsulated MBT (Supporting Information Figure 9C). Here, the drug release rates closely follow the dissolution rate of the microneedle at the 95 mol % AM and 5 mol % BAM composition employed (Figure 2).

CONCLUSIONS

In conclusion, this study has effectively shown the utility and flexibility of PISA printing for generating high-resolution 3D polymeric structures using commercially available DLP printers. A significant development in this study was the introduction of a new PISA system based on the self-assembly of acrylamide and isopropanol. This addition expands the range of materials compatible with PISA printing, including BAM to adjust aqueous dissolution kinetics. The soluble structures created had controllable aqueous dissolution rates, which proved crucial for the development of "poke and release" microneedles. These microneedles had feature sizes as low as 27 μm, almost reaching the resolution limit of the DLP printer used, and showed the potential for sustained drug delivery applications. The base of the microneedles dissolved quickly in physiological fluids, leaving behind more slowly dissolving tips. Overall, these findings support the idea that PISA Printing can serve as a robust and versatile method for creating intricate, high-resolution structures for a wide range of applications.

https://doi.org/10.1021/acsapm.3c02796
ACS Appl. Polym. Mater. 2024, 6, 1944–1950

■ ASSOCIATED CONTENT

Supporting Information

The Supporting Information is available free of charge at https://pubs.acs.org/doi/10.1021/acsapm.3c02796.

Experimental procedure for synthesis of transmer, RSS, poly(DMA) RSS; microneedle resin preparation; DLP printing/printing parameters of microneedles; dissolution studies; SEM imaging; AFM imaging; drug release studies; ^{1}H NMR in $CDCl_3$ for synthesized transmer, RSS, and poly(DMA) RSS; GPC traces for the synthesized RSS and poly(DMA) RSS; and graphs for drug release kinetics of 10CAM and MBT from cross-linked PISA resin-cured parts and MBT from un-cross-linked PISA cured parts (PDF)

■ AUTHOR INFORMATION

Corresponding Author

Anthony J. Convertine − *Materials Science and Engineering Department, Missouri University of Science and Technology, Rolla, Missouri 65409, United States;* orcid.org/0000-0002-3263-1523; Email: convertinea@mst.edu

Authors

Aaron Priester − *Materials Science and Engineering Department, Missouri University of Science and Technology, Rolla, Missouri 65409, United States*

Jimmy Yeng − *Materials Science and Engineering Department, Missouri University of Science and Technology, Rolla, Missouri 65409, United States*

Yuwei Zhang − *Chemistry Department, Missouri University of Science and Technology, Rolla, Missouri 65409, United States*

Krista Hilmas − *Joint Department of Biomedical Engineering, North Carolina State University and The University of North Carolina at Chapel Hill, Raleigh, North Carolina 27695, United States*

Risheng Wang − *Chemistry Department, Missouri University of Science and Technology, Rolla, Missouri 65409, United States;* orcid.org/0000-0001-6539-1565

Complete contact information is available at: https://pubs.acs.org/10.1021/acsapm.3c02796

Author Contributions

A.J.C. conceived the idea. A.P. synthesized RAFT macro-CTAs, performed monofunctional and photoabsorber studies, designed resin formulations, PISA printed microneedles, performed dissolution studies, and characterized the materials via NMR and UV−vis analyses. J.Y. first tested the acrylamide PISA in 91% IPA. Y.Z. and R.W. imaged the materials by AFM. K.H. synthesized the RAFT transmer and some macro-CTAs.

Funding

We would like to thank the Center for Biomedical Research (CBR) at Missouri University of Science and Technology for providing seed funding to support this work.

Notes

The authors declare no competing financial interest.

■ ABBREVIATIONS

AM, acrylamide; BAM, N-(butoxymethyl)acrylamide; HEAm, 2-(hydroxyethyl)acrylamide; DMA, N′N-dimethylacrylamide; RSS, radiant star scaffolds; DLP, digital light projection; SEM, scanning electron microscopy; AFM, atomic force microscopy; DAAm, diacetone acrylamide; RAFT, reversible addition−fragmentation chain transfer; PISA, polymer-induced self-assembly; GPC, gel permeation chromatography; CTA, chain transfer agent; LAP, lithium phenyl-2,4,6-trimethylbenzoylphosphinate; DMF, N′N-dimethylformamide; PEG, poly(ethylene glycol); DP, degree of polymerization; 10CAM, 10-hydroxycamptothecin; MBT, methylene blue trihydrate; MBAc, N′*N*-methylenebis(acrylamide); BTP, 2-(butylthiocarbonothioylthio)propanoic acid; PIMS, polymerization-induced microphase separation

■ REFERENCES

(1) Maines, E. M.; Porwal, M. K.; Ellison, C. J.; Reineke, T. M. Sustainable advances in SLA/DLP 3D printing materials and processes. *Green Chem.* **2021**, *23*, 6863−6897.

(2) Amini, A.; Guijt, R. M.; Themelis, T.; De Vos, J.; Eeltink, S. Recent developments in digital light processing 3D-printing techniques for microfluidic analytical devices. *J. Chromatogr., A* **2023**, *1692*, No. 463842.

(3) Gojzewski, H.; Guo, Z.; Grzelachowska, W.; Ridwan, M. G.; Hempenius, M. A.; Grijpma, D. W.; Vancso, G. J.; Layer-by-Layer Printing of Photopolymers in 3D: How Weak is the Interface? Appl, A. C. S. *Mater. Interfaces* **2020**, *12*, 8908−8914.

(4) Sun, C.; Fang, N.; Wu, D. M.; Zhang, X. Projection micro-stereolithography using digital micro-mirror dynamic mask. *Sens. Actuators, A* **2005**, *121*, 113.

(5) Bagheri, A.; Jin, J. Photopolymerization in 3D Printing. *ACS Appl. Polym. Mater.* **2019**, *1*, 593.

(6) Di Lorenzo, F.; Seiffert, S. Nanostructural heterogeneity in polymer networks and gels. *Polym. Chem.* **2015**, *6*, 5515.

(7) Jenkins, A. D.; Jones, R. G.; Moad, G. Terminology for reversible-deactivation previously called "controlled" radical or "living" radical polymerization (IUPAC Recommendations 2010). *Pure Appl. Chem.* **2009**, *82*, 483−491.

(8) Li, J.; Boyer, C.; Zhang, X. 3D Printing based on Photopolymerization and Photocatalysts: Review and Prospect. *Macromol. Mater. Eng.* **2022**, *307*, No. 22000210.

(9) Zhang, Z.; Corrigan, N.; Bagheri, A.; Jin, J.; Boyer, C. A Versatile 3D and 4D Printing System through Photocontrolled RAFT Polymerization. *Angew. Chem., Int. Ed.* **2019**, *58*, 17954−17963.

(10) Semsarilar, M.; Abetz, V. Polymerizations by RAFT: Development of the Technique and Its Application in the Synthesis of Tailored (Co)polymers. *Macromol. Chem. Phys.* **2020**, *222*, No. 2000311.

(11) Bagheri, A.; Engel, K. E.; Bainbridge, C. W. A.; Xu, J.; Boyer, C.; Jin, J. 3D printing of polymeric materials based on photo-RAFT polymerization. *Polym. Chem.* **2020**, *11*, 641−647.

(12) Zhao, B.; Li, J.; Xiu, Y.; Pan, X.; Zhang, Z.; Zhu, J. Xanthane-Based Photoiniferter RAFT Polymerization toward Oxygen-Tolerant and Rapid Living 3D Printing. *Macromolecules* **2022**, *55*, 1620−1628.

(13) Maruyama, T.; Mukai, M.; Sato, R.; Iijima, M.; Sato, M.; Furukawa, T.; Maruo, S. Multifunctional 3D Printing of Heterogeneous Polymer Structures by Laser-Scanning Micro-Stereolithography Using Reversible-Addition Fragmentation Chain-Transfer Polymerization. *ACS Appl. Polym. Mater.* **2022**, *4*, 5515−5523.

(14) Shi, X.; Zhang, J.; Corrigan, N.; Boyer, C. PET-RAFT facilitated 3D printable resins with multifunctional RAFT agents. *Mater. Chem. Front.* **2021**, *5*, 2271−2282.

(15) Lee, K.; Corrigan, N.; Boyer, C. Rapid High-Resolution 3D Printing and Surface Functionalization via Type I Photoinitiated RAFT Polymerization. *Angew. Chem., Int. Ed.* **2021**, *60*, 8839.

(16) Zhao, B.; Li, J.; Pan, X.; Zhang, Z.; Jin, G.; Zhu, J. Photoinduced Free Radical Promoted Cationic RAFT Polymerization toward "Living" 3D Printing. *ACS Macro Lett.* **2021**, *10*, 1315−1320.

(17) Priester, A.; Yeng, J.; Zhang, Y.; Wang, R.; Convertine, A. J. 3D printing soluble solids via PISA. *Polym. Chem.* **2023**, *14* (20), 2452−2456.

(18) Bobrin, V. A.; Yao, Y.; Shi, X.; Xiu, X.; Zhang, J.; Corrigan, N.; Boyer, C. Nano-to macro-scale control of 3D printed materials via polymerization induced microphase separation. *Nat. Commun.* **2022**, *3*, 3577.
(19) Bobrin, V. A.; Lee, K.; Zhang, J.; Corrigan, N.; Boyer, C. Nanostructure Control in 3D Printed Materials. *Adv. Mater.* **2021**, *34* (4), No. 2107643.
(20) Wang, X.; Shi, Y.; Graff, R. W.; Cao, X.; Gao, H. Synthesis of Hyperbranched Polymers with High Molecular Weight in the Homopolymerization of Polymerizable Trithiocarbonate Transfer Agent without Thermal Initiator. *Macromolecules* **2016**, *49* (17), 6471−6479.
(21) Zhang, X. W.; Rieger, J.; Charleux, B. Effect of the solvent composition on the morphology of nano-objects synthesized via RAFT polymer- ization of benzyl methacrylate in dispersed systems. *Polym. Chem.* **2012**, *3*, 1502−1509.
(22) Zhang, X. W.; Boisse, S.; Bui, C.; Albouy, P. A.; Brulet, A.; Li, M. H.; Rieger, J.; Charleux, B. Amphiphilic liquid-crystal block copoly- mer nanofibers via RAFT-mediated dispersion polymerization. *Soft Matter* **2012**, *8*, 1130−1141.
(23) Xiao, X.; He, S.; Dan, M.; Su, Y.; Huo, F.; Zhang, W. Brush macro-RAFT agent mediated dispersion polymerization of styrene in the alco- hol/water mixture. *J. Polym. Sci. A: Polym. Chem.* **2013**, *51*, 3177−3190.
(24) Li, Q.; Huo, F.; Cui, Y.; Gao, C.; Li, S.; Zhang, W. Doubly thermoresponsive brush-linear-linear ABC triblock copolymer nanoparticles prepared through dispersion RAFT polymerization. *J. Polym. Sci. A: Polym. Chem.* **2014**, *52*, 2266−2278.
(25) Huo, F.; Li, S. T.; He, X.; Shah, S. A.; Li, Q. L.; Zhang, W. Q. Disassembly of block copolymer vesicles into nanospheres through vesicle medi- ated RAFT polymerization. *Macromolecules* **2014**, *47*, 8262−8269.
(26) Li, Q. L.; Gao, C. Q.; Li, S. T.; Huo, F.; Zhang, W. Q. Doubly thermo-responsive ABC triblock copolymer nanoparticles prepared through dispersion RAFT polymerization. *Polym. Chem.* **2014**, *5*, 2961−2972.
(27) Shi, P.; Zhou, H.; Gao, C.; Wang, S.; Sun, P.; Zhang, W. Macro-RAFT agent mediated dispersion copolymerization: a small amount of solvophilic co-monomer leads to a great change. *Polym. Chem.* **2015**, *6*, 4911−4920.
(28) Semsarilar, M.; Jones, E. R.; Blanazs, A.; Armes, S. P. Efficient synthesis of sterically stabilized nano-objects via RAFT dispersion polymer- ization of benzyl methacrylate in alcoholic media. *Adv. Mater.* **2012**, *24*, 3378−3382.
(29) Jones, E. R.; Semsarilar, M.; Blanazs, A.; Armes, S. P. Efficient synthesis of amine-functional diblock copolymer nanoparticles via RAFT dis- persion polymerization of benzyl methacrylate in alcoholic media. *Macromolecules* **2012**, *45*, 5091−5098.
(30) Zehm, D.; Ratcliffe, L. P. D.; Armes, S. P. Synthesis of diblock copolymer nanoparticles via RAFT alcoholic dispersion polymerization: effect of block copolymer composition, molecular weight, copolymer concentration, and solvent type on the final particle morphology. *Macromolecules* **2013**, *46*, 128−139.
(31) Semsarilar, M.; Ladmiral, V.; Blanazs, A.; Armes, S. P. Poly(methacrylic acid)-based AB and ABC block copolymer nanoobjects pre- pared via RAFT alcoholic dispersion polymerization. *Polym. Chem.* **2014**, *5*, 3466−3475.
(32) Gonzato, C.; Semsarilar, M.; Jones, E. R.; Li, F.; Krooshof, G. J. P.; Wyman, P.; Mykhaylyk, O. O.; Tuinier, R.; Armes, S. P. Rational synthesis of low-polydispersity block copolymer vesicles in concentrated solu- tion via polymerization-induced self-assembly. *J. Am. Chem. Soc.* **2014**, *136*, 11100−11106.
(33) Pei, Y.; Lowe, A. B. Polymerization-induced self-assembly: ethanolic RAFT dispersion polymerization of 2-phenylethyl methacrylate. *Polym. Chem.* **2014**, *5*, 2342−2351.
(34) Pei, Y. W.; Dharsana, N. C.; Van Hensbergen, J. A.; Burford, R. P.; Roth, P. J.; Lowe, A. B. RAFT dispersion polymerization of 3-phenylpropyl methacry- late with poly 2-(dimethylamino)ethyl methacrylate macro-CTAs in ethanol and associated thermoreversible polymorphism. *Soft Matter* **2014**, *10*, 5787−5796.
(35) Pei, Y.; Dharsana, N. C.; Lowe, A. B. Ethanolic RAFT dispersion poly- merization of 2-(naphthalen-2-yloxy)ethyl methacrylate and 2-phenoxyethyl methacrylate with poly[2-(dimethylamino)-ethyl methacrylate]-chain transfer agents. *Aust. J. Chem.* **2015**, *68*, 939−945.

https://doi.org/10.1021/acsapm.3c02796
ACS Appl. Polym. Mater. 2024, 6, 1944−1950